Nanoscale

Accepted Manuscript

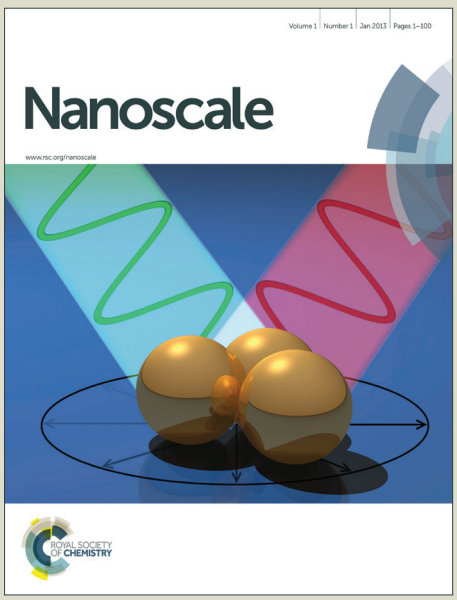

ROYAL SOCIETY OF CHEMISTRY

www.rsc.org/nanoscale

Nanoscale

RSCPublishing

ARTICLE

Highly luminescent and cytocompatible cationic Ag_2S NIR-emitting quantum dots for optical imaging and gene transfection

Cite this: DOI: 10.1039/x0xx00000x

Fatma Demir Duman,[a] Ibrahim Hocaoglu,[a] Deniz Gulfem Ozturk,[b] Devrim Gozuacik,[b] Alper Kiraz[a,c] and Havva Yagci Acar[*,a,d,e]

Received 00th January 2012,
Accepted 00th January 2012

DOI: 10.1039/x0xx00000x

www.rsc.org/

Development of non-toxic theranostic nanoparticles capable of delivering a therapeutic cargo and providing a means for diagnosis is one of the most challenging tasks in front of the nano-biotechnology. Gene therapy is a very important mode of therapy and polyethyleneimine (PEI) is one of the most successful vehicles for gene transfection, yet pose a significant toxicity. Optical imaging utilizing quantum dots is one of the newer but fast growing diagnostic modality, which requires non-toxic, highly luminescent materials, preferentially active in the near infrared region. Ag_2S NIRQDs fit to this profile perfectly. Here, we demonstrate the aqueous synthesis of cationic Ag_2S NIRQDs with a mixed coating of 2-mercaptopropionic acid (2MPA) and PEI (branched, 25 kDa), that are highly luminescent in the NIR-I window (λ_{em} = 810-840 nm) as new theranostic nanoparticles. Synergistic stabilization of QD surface via simultaneous use of a small molecule and a polymeric material provided the highest quantum yield, 150 % (with respect to LDS 798 at pH 7.4), reported in the literature for Ag_2S. These cationic particles show dramatic improvement in cytocompatibility even without PEGylation, strong optical signal easily detected by confocal laser microscopy and effective conjugation and transfection of green fluorescence protein plasmid (pGFP) to HeLa and MCF-7 cell lines (40 % efficiency). Overall, these Ag_2S NIRQDs demonstrate great potential as new theranostics.

Introduction

Gene therapy has emerged as a very promising method in the fight against genetic disorders. The major issue in gene therapy is the safe delivery of the gene to target. Potential gene vectors should condense and protect nucleic acids effectively.[1] So far, two major approaches utilized in nucleic acid delivery are the use of viral and non-viral delivery vectors. Safety hazards of viral vectors remain as a big handicap despite of their high transfection efficiency. Non-viral vectors are usually cationic liposomes, dendrimers or polymers.[2-5] One of the best performing synthetic materials is known as polyethyleneimine (PEI). PEI can easily penetrate into cells and disrupt endosomal organelles due to the "proton sponge effect" and release its cargo.[6-8] Transfection efficiency of PEI is molecular weight dependent and increases with increasing molecular weight yet, high molecular weight PEI has significant toxicity as well. So, dosing requires a critical balance of these two factors.[9]

Semiconductor quantum dots (QD) are the new class of fluorescent probes for cellular, molecular and *in-vivo* imaging applications, due to their stable and size-tunable fluorescence. Narrow emission, broad absorption window, large molar extinction coefficient, and high chemical stability are also major advantages of QDs over organic fluorophores which make them promising optical imaging agents.[10-12] Majority of the examples in the literature involve QDs with luminescence in the visible region. However, in the visible window photons are scattered and absorbed by biological constituents such as hemoglobin. Near-infrared (NIR) fluorescence is most favorable for biological applications since it provides a higher penetration depth into the tissues than visible light, lower background fluorescence, lower signal loss, thus a greater signal to background ratio.[13, 14] The absorption by biological constituents is minimal between 700-1300 nm and QDs emitting in this region are by far more advantageous for biological applications, especially for in vivo imaging.[15-18] Such potential accelerated the development of NIR-emitting quantum dots such as PbSe,[19] PbS,[20] CdHgTe.[21] However, the intrinsic toxicity of Pb, Cd, or Hg is a significant limitation.[22] Therefore, biocompatible NIRQDs would be best suited as optical imaging agents and Ag_2S NIRQDs seems to satisfy this requirement.[23-30] Ag_2S show a low release of Ag^+ ion rendering it highly cytocompatible.[24, 31] Wang et al. produced hydrophobic Ag_2S NIRQDs emitting at 1058 nm from $(C_2H_5)_2NCS_2Ag$[32] and then the PEGylated ones via ligand exchange with DHLA and conjugation with PEG. This Ag_2S NIRQDs emitting at 1200 nm showed enhanced spatial resolution in the *in vivo* imaging of angiogenesis[33] and allowed tracking of mesenchymal stem cells *in vivo*.[34] In the last four years there has been a tremendous amount of effort in aqueous synthesis of Ag_2S NIRQDs. Tian et al. synthesized water-soluble Ag_2S quantum dots coated with 3-mercaptopropionic acid and demonstrated its use as an optical probe in the *in vivo* studies using mice.[23] Cui and Su et al. synthesized Ag_2S NIRQDs using RNase A as template in aqueous medium via biomimetic route.[24]

Pang et al. prepared emission-tunable Ag_2S quantum dots in a two-step procedure.[25] Yan et al. reported bovine serum albumin (BSA)-stabilized NIR emitting Ag_2S NIRQDs and its conjugation with endothelial growth factor (VEGF) antibody for targeted cancer imaging.[26] Wang et al. studied long-term *in vivo* effect and biodistribution of PEGylated-Ag_2S NIRQDs. The prepared QDs accumulated in the RES (reticuloendothelial system), especially in the liver and spleen and cleared from the body by fecal excretion.[27] Hocaoglu and Acar reported one of the first examples of simple aqueous synthesis of highly luminescent and cytocompatible Ag_2S quantum dots which were stabilized with 2-mercaptopropionic acid.[35] These Ag_2S NIRQDs have the highest QY reported in the literature so far with 39 %, upon aging. The effective imaging properties of Ag_2S NIRQDs were demonstrated in mammalian cells for the first time in the literature and enhanced cytocompatibility was shown even at extremely high doses (up to 200 µg/mL).

One of the most important factors in getting good quality QDs is the surface passivization. Packing density of the coating material on crystal surface and the binding strength are also important. Uncoordinated sides on the crystal surface may act as defects and cause non-radiative coupling events, causing relatively low luminescence intensity. As optical probes, QDs with strong luminescence are highly desirable as they would provide a better signal to noise ratio and may allow usage of lower doses. Previously, we have shown that when a mixture of a polymeric material and a small thiolated ligand were used as a coating for CdS, both the ability to tune crystal size and the quantum yield of CdS QDs has improved dramatically.[36] Also, we have demonstrated that 2MPA is a much more advantageous coating when compared to the widely used 3-MPA, in terms of stability and luminescence intensity of the resulting QDs due to the interaction of carboxylate groups to crystal surface in addition to thiol binding which was shown by ab initio calculations and supported by life time measurements.[37] Therefore, Ag_2S NIRQDs were synthesized with mixed coating of bPEI (25 kDa) and 2MPA, in order to achieve highly luminescent, stable and cationic nanoparticles.

Here, we report the development of the first NIR emitting cationic Ag_2S NIRQD-based theranostic material designed as a gene delivery vector and as an optical imaging agent. In order to achieve high transfection efficiency, low cytotoxicity, strong luminescence and cytocompatibility, mixtures of branched PEI (25 kDA) and 2MPA were utilized as the direct coating of Ag_2S nanocrystals in an aqueous synthesis procedure. In almost all related literature wherein cationic QDs are developed, PEI was either covalently attached to the Cd-chalcogenides which were initially coated with materials comprising carboxylic acid and in general were further functionalized with PEG to reduce the toxicity[11] or electrostatically bound to anionic QD surface[38, 39] or deposited on QD surface via ligand exchange of the initial fatty acid or alike coatings.[40] Yet, these approaches usually produce large size agglomerates and/or reduce the quantum yield. Besides, in addition to its advantages, PEGylation also brings about issues such as reduced functional sites for oligonucleotide binding, decreased surface charge and interfere with endosomal escape of the particles.[11] There is one report focused on the synthesis of CdS/ZnS QDs directly coated with PEI (10 kDa) in water but the luminesence is weak and the molecular weight of the PEI is low for effective transfection.[41] There are two studies that we are familiar with which incorporates NIRQDs with PEI: (1) CdPbS coated with a silica shell was electrostatically bound to PEI, but at PEI/QD ratios where agglomeration was prevented, luminesence intensity dropped dramatically.[42] These particles were not utilized for transfection of any plasmid or drug and no data on cytotoxicity was available for the comparison. (2) CdTe based quantoplexes produced by mixing mercaptoacetic acid coated CdTe, DNA and PEI and their biodistribution was studied in vivo.[43] These quantoplexes were about 200 nm in size and had very low quantum yield (15 % of Alexa Fluor 750 which has a quantum yield of 12 %). In addition, there was a significant amount of uncomplexed PEI in the formulation which is an important drawback. Therefore, achieving good quantum yield and low cytotoxicity added to good transfection efficiency, especially with non-toxic NIRQDs is extremely advantages and we achieved this with the described approach herein.

We have designed these cationic NIRQDs with a cytocompatible NIR emitting QD core which is Ag_2S, kept the crystal size small in order to obtain emission in the NIR-I window which is suitable for fluorescence imaging in vitro using a confocal microscope, used the golden standard of synthetic transfection agents which is the 25 kDa branched PEI, but mixed it with a stable and effective 2MPA to enhance luminesence efficiency and balance the toxicity coming from the cationic coating without PEGylation. Also, this strategy allowed us to synthesize these particles directly in aqueous solutions which eliminated ligand exchange steps. The influence of reaction variables such as coating type, PEI/2MPA ratio, pH and reaction time on the optical properties of the QDs was studied systematically. Aq. Ag_2S with the highest reported quantum yield was obtained under optimized conditions of synthesis. These are also the first cationic Ag_2S NIRQDs in the literature. Cytocompatibility of these cationic Ag_2S QDs were evaluated using HeLa cell lines. Suitability of particles for imaging was demonstrated in the HeLa and MCF-7 cell lines using confocal laser microscopy. Potential of these particles as gene vectors were tested in *in vitro* transfection experiments. Transfection efficiency of PEI-2MPA coated Ag_2S NIRQDs was determined in HeLa and MCF-7 cells using green fluorescence protein plasmid (pGFP) and results were compared with a standard transfection agent (25 kDa PEI) in its standard procedure in a standard protocol. This is the first example to gene transfection and optical imaging performed with Ag_2S NIRQD, *in vitro*.

Materials and Methods

Materials

All reagents were analytical grade or the highest purity. Silver nitrate ($AgNO_3$) was purchased from Sigma-Aldrich. Sodium sulfide (Na_2S) was purchased from Alfa-Aesar. Branched polyethyleneimine (PEI) (Mw 25 kDa) was purchased from Aldrich (Germany). Linear PEI (25 kDa) was purchased from PolySciences, Inc (USA). Sodium hydroxide (NaOH), 2-mercaptopropionic acid (2MPA), ethanol and acetic acid (CH_3COOH) were purchased from Merck (USA). LDS 798 Near-IR laser dye was purchased from Exciton, Inc (USA). Only Milli-Q water (18.2 M Ohm) was used

when necessary. DMEM medium (with 4500 mg/L glucose, 4.0 mM L-glutamine, and 110 mg/L sodium pyruvate), trypsin-EDTA, penicillin-streptomycin and fetal bovine serum were purchased from HyClone, USA. Thiazolyl blue tetrazolium bromide (MTT) *Biochemica* was purchased from AppliChem, Germany. Paraformaldehyde solution 4 % in PBS and UltraCruz™ 96 well plates were purchased from Santa Cruz Biotechnology, Inc., USA. Glass bottom dishes were purchased from MadTek, USA. Dimethyl sulfoxide Hybri-Max™ and phosphate buffered saline (pH 7.4) were purchased from Sigma, USA.

Preparation of PEI and 2MPA coated Ag_2S Nanoparticle

All reactions were performed under an inert atmosphere. Typically, 42.5 mg of $AgNO_3$ (0.25 mmol) and 4.9 mg Na_2S (0.0625 mmol) were dissolved in 75 ml and 25 mL of deoxygenated water respectively in separate round bottom flasks. PEI and 2MPA in desired ratios, as listed in Table 1, were added to the $AgNO_3$ solution, respectively. Total coating/Ag mole ratio kept constant at 5. For 2MPA, moles of thiol groups and for PEI moles of amine groups were considered. As an example, a mixed coating containing 20% 2MPA, had 1 equivalent of thiol (0.25mmol) and 4 equivalents of amine (1 mmol) with respect to Ag. The pH of the final solution was adjusted using NaOH and CH_3COOH solutions (2.5 M). Na_2S solution was added to this reaction mixture under vigorous mechanical stirring at 5000 rpm and at room temperature (25 ^oC). During the reaction, samples were taken at different time points to follow the particle growth. Prepared quantum dot solutions were washed with deionized water using Amicon-Ultra centrifugal filters (30000 Da cut off) and stored in the dark at 4 ^oC.

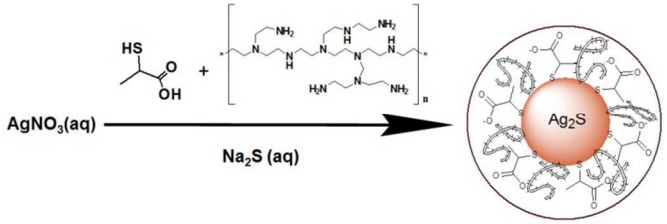

Scheme 1 Aqueous synthesis of PEI and 2MPA coated Ag_2S NIRQDs

Characterization Methods

Absorbance spectra of the prepared Ag_2S quantum dots were recorded by a Shimadzu 3101 PC UV-Vis-NIR spectrometer in the 300-1100 nm range. Crystal sizes of Ag_2S nanoparticles were calculated from absorption spectra of the particles using absorption edge in the Brus equation (Equation 1):

$$\Delta E = \frac{\hbar^2\pi^2}{8R^2}\left[\frac{1}{m_e}+\frac{1}{m_h}\right]-1.8\frac{e^2}{\varepsilon_{Ag_2S}4\pi\varepsilon_0 R} \qquad (1)$$

Where R is the radius of the nanocrystal, m_e (0.286 m_0) and m_h (1.096) are the respective effective electron and hole masses for inorganic core, and ε_{Ag2S} (5.95) is the dielectric constant and ΔE is the band gap energy difference between the bulk semiconductor and the nanocrystal.

A homemade set up was used in the photoluminescence measurements. Ag_2S NIRQDs were excited with a frequency doubled output of a DPSS laser (532 nm). After the luminescence was filtered by 590 nm long pass filter, it was collected with a 1/8 Newport Cornerstone 130 monochromator having 6001/mm grating and operating in 400-1000 nm range. The wavelength selected signals were detected by a femtowatt sensitive Si detector (Thorlabs PDF10A, 1.4 x 10^{-15} W/$Hz^{1/2}$).

For Quantum Yield (QY) calculations, QD samples in water and a NIR dye in methanol were prepared at five different concentrations having absorbance values at the excitation wavelength at and below 0.15. These five concentrations were adjusted in such a way that absorbance values of the dye samples and QD samples are close to each other. LDS 798 NIR dye (quantum yield reported as 14 % in MeOH by the producer) was used as the reference. Photoluminescence of these solutions were recorded at excitation wavelength of 532 nm, and the integrated areas under the curves were plotted against the absorbance (Fig. S1 and S2). QY was calculated from the ratio of the slope of these plots, using the refractive index of the water and MeOH based on equation 2, as reported in the literature.[36, 44, 45]

$$\Phi_{QD} = \left(\frac{Grad_{QD}}{Grad_{REF}}\right)\left(\frac{\eta_{water}^2}{\eta_{MeOH}^2}\right)\times 100 \qquad (2)$$

The XRD pattern of the quantum dots was recorded between 2θ angles of 10^o and 90^o using a Bruker D2 Phaser Benchtop XRD system with Cu K-α radiation (λ=1.5406 A^o). About one gram of dried sample was placed in between gelatine film. Air bubbles were removed and the sample was placed on a sample holder. TEM analysis of nanoparticles was performed using a JEOL JEM-ARM200CFEG UHR-Transmission Electron Microscope (JEOL, Japan). The hydrodynamic size and zeta potential of the aqueous nanoparticles were measured with a Malvern Zetasizer Nano-ZS. A Thermo Scientific K-Alpha XPS with Al K-alpha monochromatic radiation (1486.3 eV) was used for XPS analysis of QDs. Dried samples were placed on adhesive aluminum tape. A 400 µm x-ray spot size and 50.0 eV pass energy corresponding to a resolution of roughly 0.5 eV were used. The base pressure and experimental pressure were below 3×10^{-9} mbar and about 1×10^{-7} mbar. C1s peak at 285.0 eV was assigned as the reference signal for evaluations.

Ag^+ concentration of QD solutions was determined by Spectro Genesis FEE Inductively Coupled Plasma Optical Emission Spectrometer (ICP OES). QDs were exposed to acids (suprapur nitric acid 65 % and suprapur sulphuric acid 96 %) for digestion and diluted to certain volumes. Ag^+ ion concentrations in solutions were calculated using a standard curve of known Ag^+ ion concentrations.

Cell lines, cell culture

MCF-7 human breast carcinoma and HeLa cell lines were cultured in DMEM (Sigma, 05671) supplemented with 10% (v/v) fetal bovine serum (FBS; Biochrom KG, S0115) and antibiotics

(Penicillin/Streptomycin; Biological Industries, 03-031-1B) in a 5% CO_2-humidified incubator at 37°C.

Gene delivery tests

Ag_2S-PEI-2MPA mediated transfections were conducted by mixing various concentrations of QDs (according to measured concentrations of Ag^+ ions by ICP OES) (1 µg/ml, 1.5 µg/ml, 2 µg/ml and 2.5 µg/ml) with 4 µg pMax-GFP vector DNA (Lonza) in 50 µl serum-free DMEM. Mixtures were allowed to incubate for 10 min and were added to cells seeded in 12-well plates (MCF-7: 100.000 cells/well, HeLa: 75.000 cells/well). After six hours post-transfection, cells were washed with PBS and fresh medium was added. Control transfections were conducted similarly, using the linear 25 kDa polyethyleneimine (PEI) (1 µg/ml) as one of the standard transfection agents.

Transfection efficiency was checked 48 h post-transfection. Prior to analysis, cell nuclei were stained with the Hoechst dye (Invitrogen, 33342) to better assess the ratio of GFP positive cells to the total cell population. Hoechst was added to the cells at a final concentration of 1µg/ml. After 20 minutes incubation, cells were washed with PBS to remove excess amount of dye. Cells were fixed in 3.7 % paraformaldehyde for 20 min, washed with PBS, mounted in 50% glycerol in PBS and inspected under 20x or 40x magnification using an BX60 fluorescence microscope (Olympus). At least 150 cells per condition were analyzed and results were expressed as a percentage of GFP positive cells versus total number of cells (Hoechst dye positive nuclei). All measurements were repeated in at least 3 independent experiments.

Cytotoxicity Assay

To study the cytotoxicity of the prepared QDs on the HeLa cells lines, thiazolyl blue tetrazolium bromide (3-(4,5-dimethyl-thiazol-2yl)-2,5-diphenyltetrazolium bromide, MTT) was utilized. Cells were cultured in the 96-well plates with complete medium at 37 ^oC and 5 % CO_2 for 24 h. On the second day, the medium was renewed and QDs were added to the culture medium at different concentrations and incubated for another 24 h. On the third day, cells were washed with PBS. MTT reaction solution was added on the cells and incubated for 4 h. Purple formazan was dissolved with DMSO : Ethanol (1:1) by gentle shaking for 15 min. Absorbance of formazan was measured by reading absorbance at a wavelength of 600 nm with a reference at 630 nm on a microplate reader (BioTek ELx800 Absorbance Microplate Reader). QD absorbance in a complete medium was measured as well and subtracted from the MTT solution to correct the result. Experiments were repeated four times. Statistical analysis was performed with GraphPad Prism Software (Graphpad Software, Inc., USA). Columns were compared as pairs by Tukey's multiple comparison test of one way ANOVA test with Tukey's multiple comparison test or by using a two tailed student's t-test. All data were represented as mean ± SD (standard deviation). The confidence level was accepted as 95 % (significant at $p < 0.05$).

Cell Imaging

Imaging of HeLa and MCF-7 cells was performed using two different confocal laser scanning microscopes in order to visualize NIR emission of QDs and GFP signal. For QD localization analysis, 50.000 HeLa cells were cultured in glass bottom dishes and incubated for 18 h. Following incubation, the culture medium was replenished and cells were incubated with QD solution which has 2.5 µg/mL of Ag^+ ion for 6 h. Cells were washed with PBS (pH 7.2) and fixed with 4 % paraformaldehyde for 15 min. Finally, the washing step was repeated and cells were kept in PBS to protect the cells from drying. To detect intracellular uptake and localization of Ag_2S NIRQD, a home-made sample scanning confocal microscope system equipped with Si avalanche photodetector and a 60X (NA : 1.49) oil immersion objective was used. Excitation laser beam at 532 nm was transmitted through neutral density filters and reflected by a broadband dichroic mirror (Chroma 10/90 beamsplitter). A long pass glass filter RG665 was placed before the detectors to collect the QD emission.

Confocal laser microscopy studies performed to visualize the green fluorescence in transfected cells by GFP/Ag_2S NIRQDs. Initially, 150.000 MCF-7 or HeLa cells were cultured in 12-well plates with cover slides. After overnight incubation, transfection with a QD solution (at concentration of 2.5 µg/mL of Ag^+) conjugated to pMax-GFP plasmid was performed. Cells were washed with PBS after 6 hours of incubation. At 48 hours after transfection, cells were fixed in 3.7 % paraformaldehyde for 20 min, washed with PBS and mounted in 50 % glycerol in PBS. Cells were imaged using a Nikon Eclipse Te2000-U confocal microscope to detect the GFP signal after transfection.

Results and Discussion

PEI coated NIR-emitting Ag_2S Quantum Dots

Direct aqueous synthesis was utilized in the synthesis of cationic NIR-emitting Ag_2S NIRQDs as a greener and a facile synthesis method. Cationic Ag_2S NIRQDs were synthesized directly in water from $AgNO_3$ and Na_2S under inert atmosphere at room temperature with branched PEI (25 kDa), as a coating. Factors that usually affect the particle size and the quality such as reaction duration, Ag/S and PEI/Ag ratio were studied to investigate the ability to tune size and therefore, the emission wavelength of QDs, and to find out the conditions which would produce the best luminescing particles within the 700-900 nm range. The pH of the reaction solution was around 9-10 due to the presence of PEI. Results indicated that PEI can stabilize QDs in the aq. medium; however, these variables did not allow efficient size tuning and the luminescence of the particles were poor (Fig. S3 and S4). In polymer coated particles, due to the lack of dense packing on the particle surface, a significant amount of defects may exist resulting in non-radiative coupling events and hence, low luminescence.

PEI/2MPA coated NIR-emitting Ag_2S Quantum Dots

In order to improve the luminescence quality of Ag_2S NIRQDs and achieve size tunability, mixed coating formulations composed of PEI and 2MPA were used. Ag_2S NIRQDs with only 2MPA coating was

also prepared for comparison of the properties. All particles were synthesized under identical conditions (Table 1). Usually, reaction time allowed for the crystal growth may act as a factor in tuning particle size. However, initial experiments done with 100 % PEI and 60/40 PEI/2MPA have shown that particle size or luminescence peak maximum of resulting QDs does not change after 5 min (Fig. S5) following the addition of Na_2S. Therefore, all comparative reactions were quenched in liq. nitrogen at 5 min after sulfide addition.

In the QD synthesis, pH of the reaction mixture was adjusted to 10 before the addition of Na_2S, except in the case of 100 mol % 2MPA which was performed at pH 7.5, since Ag-2MPA complex precipitates at higher pH values. The pH of the PEI solution is usually around 10, but after the addition of 2MPA to the reaction mixture, a significant drop in pH was observed. As an example, pH drops to 7.5 - 7.8 with 20 mol % 2MPA, and to 3.0-3.5 in the case of 40 mol % 2MPA. pK_a of PEI is in the range of 8.2 to 9.5.[46-48] Protonation of the amines is problematic since they will be responsible from the binding of PEI to the QD surface. Thus, pH was readjusted to 10 before the addition of the sulfur source to the reaction mixture.

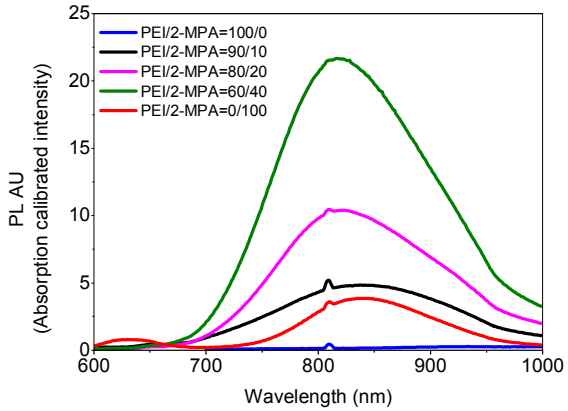

Fig. 1. Photoluminescence spectra of Ag_2S NIRQDs prepared with different PEI/ 2MPA ratios (Ag: S = 4, room temperature, reaction pH: 10, 5 min reaction).

In comparable reactions in which Ag/S ratio and coating/Ag ratio were set at 4 and 5, respectively, only the PEI/2MPA ratio was changed to study the influence of coating composition on particle properties. All reactions with up to 40 mol % 2MPA formed stable colloidal suspension of QDs with a dramatically improved luminescence intensity over the ones with 100 mol % PEI coating (Fig. 1). Besides, these QDs also outperformed the luminescence intensity of 100 mol % 2MPA coated Ag_2S NIRQDs which were the best luminescing Ag_2S NIRQDs reported in the literature until now.[35] Amongst the PEI/2MPA coated Ag_2S NIRQDs, the best luminescence intensity was obtained with 20 and 40 mol % 2MPA in the coating mixture (Fig. 1). Non-luminescent bulk material was obtained when 60 mol % 2MPA was used. Therefore, higher 2MPA content in the mixture was not attempted. Addition of 2MPA as co-stabilizer also reduced the particle (inorganic crystal) size (Table 1). Actually, all QDs prepared with the mixed coating formulations are also smaller than 100 mol % 2MPA coated QDs with better luminescence indicating a synergy. This is in agreement with the results obtained from poly(acrylic acid)/mercaptoacetic acid coated CdS QDs.[36, 49] In case of polymeric coatings, the lack of dense surface passification causes poor control in crystal growth and poor surface quality resulting in large crystals with surface defects possibly responsible from nonradiative couplings reducing the quantum yield and the luminescence intensity. Addition of a small thiolated ligand which binds strongly and densely to the surface left uncapped by the polymeric coating both limits crystal growth more effectively and reduce surface defects. As a result, mixed coatings produce smaller particles with better luminescence intensity. Increasing 2MPA amount decreased the crystal size slightly, causing a slight blue shift in the emission peak (Fig. 1, Table 1). Overall, all Ag_2S NIRQDs with mixed coating emit between 817-838 nm, which is within the so called diagnostic window, with a full-with-at half maximum (FWHM) around 170 nm and better luminescence than 2MPA or PEI coated particles.

Table 1 Effect of PEI/2MPA ratios on the properties of Ag_2S NIRQDs

Rxn Code	PEI (%)[a)]	2MPA (%)[a)]	Rxn pH	λ_{abs}[b)] (nm)	Size[c)] (nm)	Band gap E (eV)	$\lambda_{em\ (max)}$ (nm)	FWHM (nm)	Dh[d)] (nm)	Zeta pot. (mV)
1	100	0	10	906	2.94	1.37	-	-	4.0	51
2	90	10	10	674	2.23	1.48	838	175	2.9	34
3	80	20	10	761	2.48	1.63	819	173	3.5	28
4	60	40	10	777	2.52	1.60	817	168	3.8	36
5	0	100	7.5	806	2.61	1.54	837	128	7.10	-62

[a)] Mol %; [b)] Absorbance onset measured from absorbance spectrum (Figure S6 [c)] Diameter of Ag_2S crystal calculated by Brus equation; [d)] Hydrodynamic diameter measured by DLS at pH 7.4 and reported as the number average. All reactions were quenched in 5 min.

Journal Name RSCPublishing

COMMUNICATION

Ag_2S-PEI/2MPA QDs were designed as potential theranostic nanoparticles with cationic surfaces. Zeta potential of the Ag_2S-PEI is 51 mV and it drops down to -30 mV in case of Ag_2S-2MPA (Table 1). Although 2MPA decreases the cationic coating content, QDs with mixed coatings are still cationic enough (ca 30 mV) for possible use as oligonucleotide condensing vectors.

Protonation of PEI with the addition of 2MPA is an important issue. Between the pH values of 5.5 and 11 (before the addition of sulfur source) no significant change in the particle size or the position of emission maximum was observed for Ag_2S-PEI/2MPA NIRQDs with 20 and 40 mol % 2MPA in the coating composition (Fig. 2 and Fig. S7).

Influence of the pH on particle properties

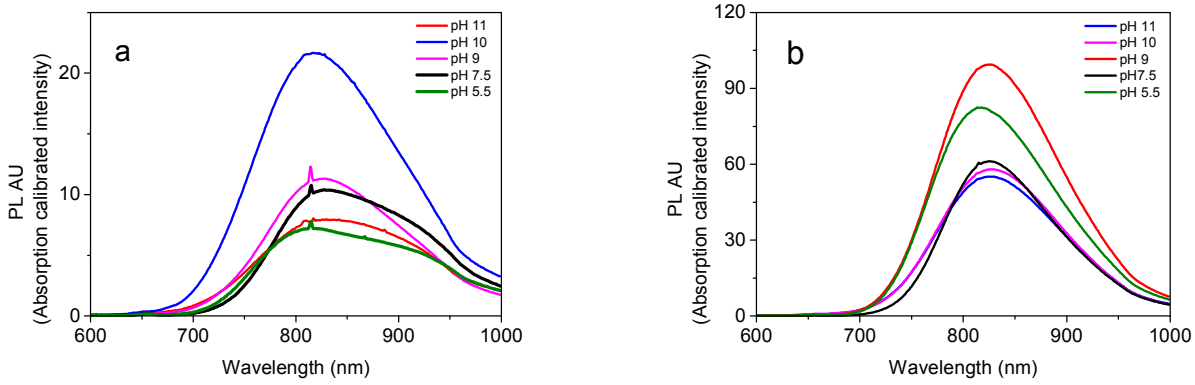

Fig. 2 Photoluminescence spectra of Ag_2S NIRQDs prepared with (a) 60/40 PEI/2MPA (Rxn 4) and (b) 80/20 PEI/2MPA (Rxn 3) coating formulation. Spectra were taken particles are washed and solution pH was adjusted to 7.4 to prevent difference in intensity based on pH.

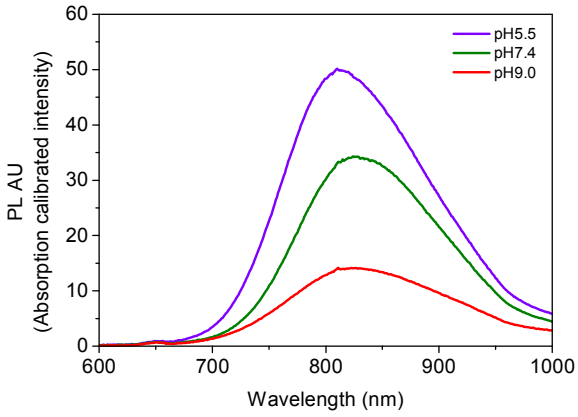

Fig. 3 Photoluminescence spectra of aqueous Ag_2S NIRQDs at different pH values. NIRQDs were prepared with 80/20 PEI/2MPA coating formulation, washed and pH was adjusted (Ag: S = 4, Ag: PEI = 1: 4, Ag: 2MPA = 1: 1, T = RT, reaction pH = 9, reaction time = 5 min).

After all, pH had a strong influence on the luminescence intensity. The best luminescence was obtained at pH 10 with 60/40 PEI/2MPA composition and pH 9 for 80/20 PEI/2MPA. In addition, emission peaks with 60/40 PEI/2MPA of Ag_2S NIRQDs has two emission maximum and have poor colloidal stability at pH values below 9. However, Ag_2S NIRQDs with 80/20 PEI/2MPA are stable and have strong emission at all pH values. With a motivation to understand the behavior of these QDs in different pH media such as physiologic media like blood (~pH 7.4) or in endosome (~pH 5.5), luminescence of Ag_2S NIRQDs with 80/20 PEI/2MPA was evaluated at pH 5.5, 7.4 and 9, after being synthesized at pH 9 and washed. As seen in Fig. 3, Fig. S8 and Table 2, luminescence peak position or absorption onset did not change much with the changes in pH within this range, which indicates that the PEI/2MPA coating provided a strong protection to the Ag_2S core.

Table 2 Influence of pH on the properties of Ag_2S-PEI/2MPA QDs.

pH	$\lambda_{abs(cutoff)}$ [a)] (nm)	Size [b)] (nm)	Band gap (eV)	$\lambda_{em(max)}$ (nm)	FWHM (nm)	Dh[c)] (nm)	Zeta pot. (mV)	QY (%)
5.5	783	2.54	1.59	812	151	9.4	63	166
7.4	783	2.54	1.59	828	150	8.9	60	150
9.0	783	2.54	1.59	825	170	8.0	32	77

[a)]Absorbance onset; [b)] Crystal diameter calculated by Brus equation; [c)] Hydrodynamic diameter measured by DLS and reported as the number average; [d)] Quantum yield calculated with respect to LDS 798 near-IR dye (Ag: S = 4, Ag: PEI = 1: 4, Ag: 2MPA = 1: 1, Temp = RT, reaction pH = 9, reaction time = 5 min).

As expected, zeta potential increased substantially with decreasing pH upon protonation of the PEI. This caused a dramatic increase in the quantum yield. There may be two factors responsible such behavior: 1) a possible disaggregation of particles upon charge repulsion; 2) elimination of free electrons which may act as a hole trap. A major jump in the QY and zeta potential was observed when pH was dropped from 9 to 7.4 where secondary amines were protonated, as well. QY was doubled reaching to a value of 150 % with respect to LDS 798 near-IR dye (quantum yield reported as 14 % by the producer). Further acidification to pH 5.5 caused an additional 10 % increase in the QY (166 %). These QYs are the highest among Ag_2S NIRQDs reported in the literature to the best of our knowledge.

Long term stability of Ag_2S-PEI/2MPA QDs

Long term colloidal and luminescence stability of QDs are crucial for practical applications. Aqueous QD suspensions were stored in refrigerator and were analyzed at extended time periods to detect any change in their size, stability or QY (Table 3). All particles stayed well dispersed in water and had no precipitation even after 1 year. During this time period, while the inorganic core size of Ag_2S NIRQDs which was measured with the Brus equation and the emission maximum stayed the same, the QY decreased to 38 % in 1-year (Fig. S9). However, this value is still as high as the highest recorded QY reported so far for Ag_2S NIRQD.[35]

Table 3 Time dependent changes in particle properties.*

Time	$\lambda_{abs(cutoff)}$ [a)] (nm)	Size[b)] (nm)	$\lambda_{em(max)}$ (nm)	FWHM (nm)	QY (%)[c)]
1st day	783	2.54	828	150	150
1st month	783	2.54	828	150	111
3rd month	783	2.54	828	150	93
9th month	783	2.54	828	150	42
1 year	783	2.54	828	150	38

*Ag_2S NIRQDs synthesized with 80/20 PEI/2MPA coating formulation at pH 9.0 was used. Sample pH was adjusted to 7.4 before measurements. [a)] Absorbance onset; [b)] Crystal diameter calculated by Brus equation; [c)] Quantum yield calculated with respect to LDS 798 near-IR dye.

Particle characterization

PEI/2MPA coated Ag_2S NIRQDs are crystalline materials having the size distribution between 2-4 nm depicted from the TEM images (Fig. 4a and 4b). Broad size distribution is also possibly responsible from broad FWHM of the emission peaks. Crystal structures of the nanoparticles were observed well in the focused images (Fig. 4c and 4d). The interplanar distance measured from the focused images is 0.221 nm and it fits well to the reported values for the 031 plane of monoclinic Ag_2S.[50, 51]

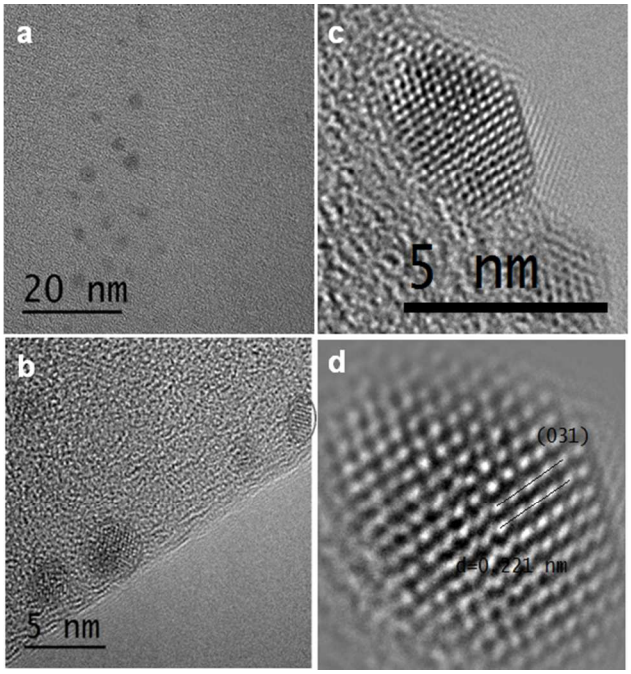

Fig. 4 TEM images of Ag_2S NIRQDs (80/20 PEI/2MPA; synthesized at pH 9.0) at different magnifications (a and b); Diffraction of Ag_2S crystal lattice (c); d-spacing determined by a focused image (d).

XRD analysis did not provide well resolved peaks due to the presence of polymer (not shown). However, XPS analysis indicates formation of Ag_2S (Fig. 5). Ag 3d core level peaks at the binding energies (BE) of 367.41 (3d5/2) and 373.45 (3d3/2) eV fits well to the Ag^+ of Ag_2S. There are two different S based on the doublets fitted to S 2p signal: S 2p3/2 at BE of 160.82 eV and 162.05 eV fits to the S-Ag and S of 2MPA, respectively[35] N 1s region can be fitted to three peaks at 398.25, 398.75 and 400.56 eV corresponding to

tertiary, secondary and primary N of PEI. Based on the literature values reported for primary amine of free PEI (399.84 eV), this shift to higher BE indicates surface binding of primary N and electron donation to QD. [52]

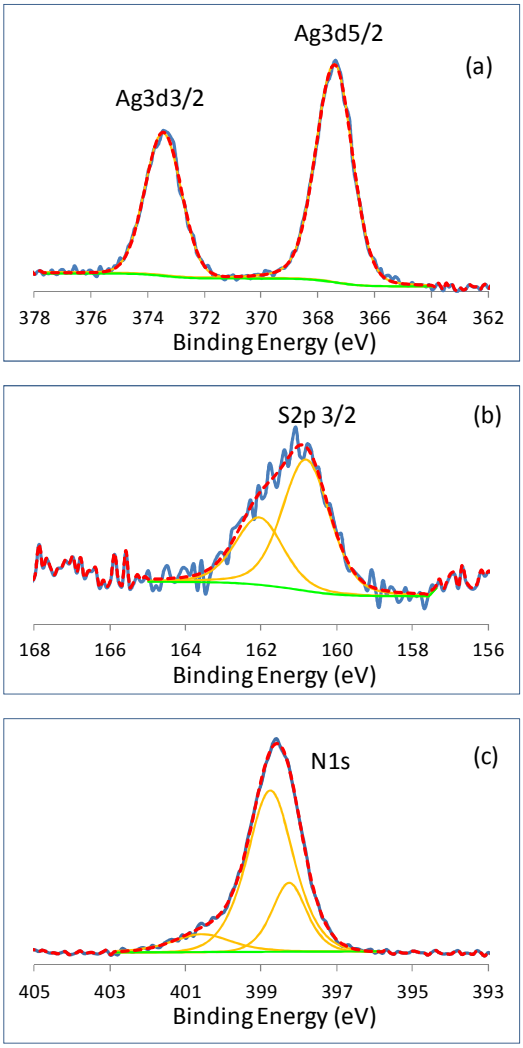

Fig. 5 (a) Ag 3d, (b) S 2p and (c) N 1s XPS spectra of Ag_2S-PEI/2MPA (80/20) QDs.

Cytocompatibility of Quantum Dots

The most stable and most strongly luminescing Ag_2S NIRQD (80/20 PEI/2MPA) was subjected to *in vitro* cytotoxicity studies. For comparison, Ag_2S-PEI and Ag_2S-2MPA NIRQDs were also subjected to same tests. Viability of HeLa cells after 24 h incubation with QDs at 1-25 µg Ag^+/mL concentrations, which correspond to 4.6-115 µg QD/mL, were determined with widely used MTT assay (Fig. 7). As seen in Fig. 6, 100 % 2MPA coated Ag_2S NIRQDs are not toxic within this dose range as expected based on previously published data[35] On the other hand, PEI (branched, 25 kDa) is known to be toxic.

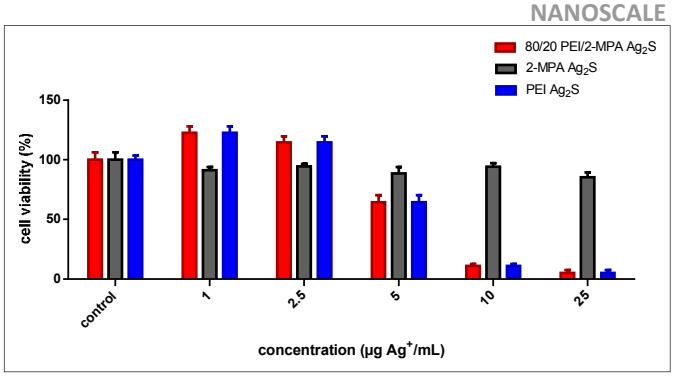

Fig. 6 Percent viability of HeLa cells exposed to Ag_2S NIRQD with PEI, 2MPA and 80/20 PEI/2MPA mixed coatings determined by MTT assay. Concentrations are based on Ag^+ ion concentration in QD solutions as determined by ICP-OES. This concentration range corresponds to 4.6-115 µg QD/mL.

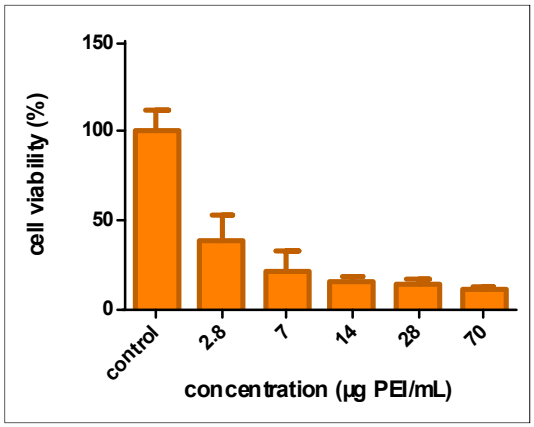

Fig. 7 Percent viability of HeLa cells exposed to PEI as determined by MTT assay. These five PEI concentrations correspond to maximum possible amount in Ag_2S NIRQDs synthesized with 80/20 PEI/2MPA coating and tested (Fig. 6). As an example, in 1.6 mg nanoparticle/mL there is 1 µg/mL Ag^+ and 2.8 µg/mL PEI.

To understand its possible contribution to NIRQD toxicity, amount of PEI coming from the formulation, was applied to the HeLa cells as well. As an example, in 4.6 µg nanoparticle/mL, there is 1 µg/mL Ag^+ (measured by ICP-OES) and 2.8 µg/mL PEI. So, for 4.6-115 µg QD/mL dose range, 2.8-70 µg/mL PEI dose range was tested (Fig. 8). Drop in the cell viability at all doses with respect to control is statistically significant ($p < 0.05$), but the differences between each concentration of PEI are insignificant. Overall, PEI was highly toxic even at the lowest dose of 2.8 µg/mL (less than 50 % viability). However, binding PEI to Ag_2S surface improved cytocompatibility dramatically with respect to free PEI. Ag_2S NIRQDs with 100 mol % PEI or 80/20 PEI/2MPA coating showed no statistically significant drop in the cell viability up to 2.5 µg Ag^+/mL, but at 5 µg Ag^+/mL viability dropped to 64 ± 12 %. Using mixed coating at given Ag^+ concentration meant a lower amount of PEI for the given dose, but the improvement over the pure PEI is much more dramatic than what this 20 % less PEI may cause. One possible reason may be the occupation of some amine groups with crystal surface binding. Considering the high cytocompatibility of 2MPA coated Ag_2S, it is

safe to say that toxicity originates from the PEI component. Looking at the similarities of PEI and PEI/2MPA coated particles in cell viability (Fig. 6), it may be reasonable to say that 2MPA did not impact viability much. 2MPA is the smaller size component of the coating mixture with a tight binding to crystal surface which is embedded in the relatively thicker PEI coating. Therefore, 2MPA did not interact with the cell, but PEI did. Therefore, at all doses, pure PEI or PEI/2MPA mixed coating resulted in similar viability levels.

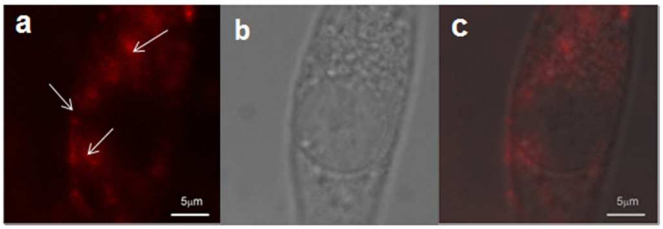

Fig. 8 Cellular uptake and localization of PEI/2MPA coated Ag_2S NIRQDs by HeLa cells. Near IR (a), transmission (b) merged image (c) of an individual cell. Red color shows the quantum dots. Arrows show some of the QDs in the cell.

Cell internalization and optical imaging

Strong emission in the NIR, cytocompatibility at low doses and effective gene delivery would make these particles excellent theranostic tools. For diagnostic purposes, strong intracellular signals originating from QDs is very important. Confocal images of the HeLa and MCF-7 cells incubated with Ag_2S NIRQDs with 80/20 PEI/2MPA indicates an efficient cell internalization and endosomal localization of QDs with strong luminescence (Fig. 8), proving potential as an optical probe. This optical signal originating from NIRQDs was dramatically stronger than the weak autofluoresence seen at this excitation wavelength (532 nm) (Fig. S11).

Use of Ag_2S-PEI/2MPA NIRQDs in the in vitro transfection

To evaluate the potential of Ag_2S NIRQDs coated with PEI/2MPA mixture as gene delivery agents, a series of *in vitro* green fluorescence protein (pMax-GFP) transfection experiments were performed with MCF-7 and HeLa cells. Commercial cell culture grade PEI (linear, 25 kDa) was used as a control. QDs were studied in a concentration range where no significant toxicity was detected ($[Ag^+]$ = 1-2.5 μg/mL, [QD] = 1-2.5 μg/mL) (Fig. 6). As shown in Fig. 9, GFP transfection efficiency and expression levels were similar or higher than the commercial PEI (used at a standard, non-toxic dose) when the GFP vector was delivered using the Ag_2S NIRQD above 1.5 μg/ml Ag^+ (6.9 μg /ml QD) concentration both in MCF-7 cells (Fig. 9) and HeLa cells (Fig. 10).

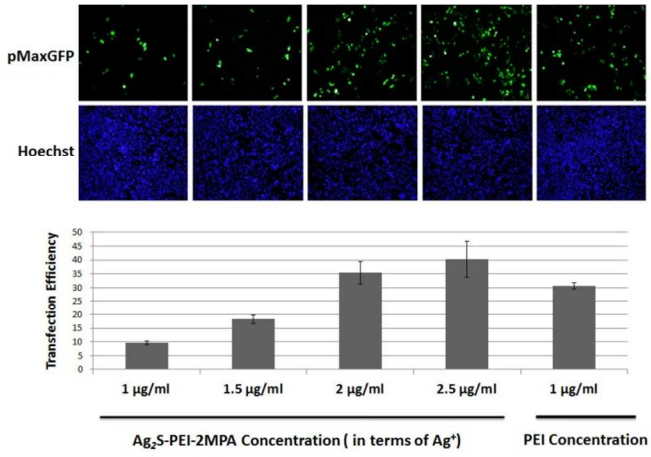

Fig. 9 Transfection of MCF-7 cells: (A) Cells were transfected with pMax-GFP plasmid using Ag_2S-PEI/2MPA NIRQD or control PEI (1 μg/ml). Transfection efficiency was assessed under a fluorescent microscope. Hoechst staining was used to show the nuclei of all cells in the field. (B) Quantitative analysis of GFP positive cells in (A) (mean ± SD of independent experiments, n = 3).

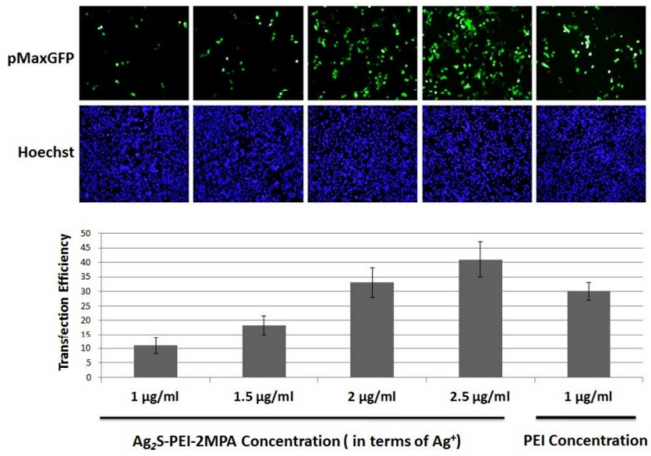

Fig. 10 Transfection of HeLa cells. (A) Cells were transfected with pMax-GFP plasmid using Ag_2S-PEI/2MPA NIRQDs or control PEI (1 μg/ml). Transfection efficiency was assessed under a fluorescent microscope. Hoechst staining was used to show the nuclei of all cells in the field. (B) Quantitative analysis of GFP positive cells in (A) (mean ± SD of independent experiments, n = 3).

Highest transfection efficiencies achieved with Ag_2S NIRQD were as 41 % for HeLa and 40 % for MCF-7 cells. Under similar conditions, transfection efficiency of commercial PEI was around 30 % for both cell lines. Considering that the actual PEI content of the QD may be lower than anticipated, and free PEI at the corresponding doses would be too toxic to be used, this improvement over free PEI may be more significant than it seems.

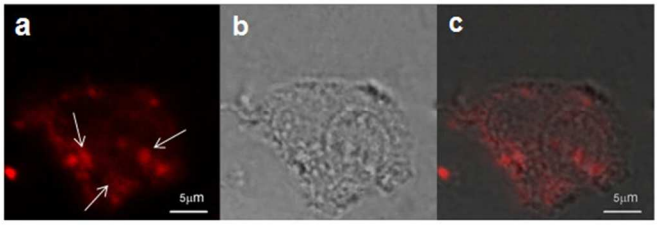

Fig. 11 Cellular uptake and localization of GFP loaded PEI/2MPA coated Ag_2S NIRQDs in MCF-7 cells. Near IR (a), transmission (b) and merged images (c) of an individual cell. Arrows show QDs in the cell.

The CLM images of the transfected MCF-7 cells with QDs (Fig. 11) demonstrate a strong optical signal originating from Ag_2S-PEI/2MPA NIRQDs proving internalization of particles conjugated with pMax-GFP by the cells. These images prove the efficient uptake of QDs with and without the plasmid. These results confirmed that both DNA binding and intact DNA delivery capabilities of Ag_2S-PEI/2MPA QDs are better than that of commercial PEI 25 kDa, promoting these QDs as biocompatible theranostic nanoparticles.

Conclusion

Theranostics have been very popular for the last decade, especially with the development of nanoparticles as drug carriers and imaging agents. Combined action of gene delivery and optical imaging is one of the most valuable capabilities in medicine and is moving towards near-infrared emitting quantum dots due to many advantages described herein. The present study demonstrated a simple, aqueous preparation of cationic, cytocompatible Ag_2S quantum dots with utilization of PEI and 2MPA mixed coatings and their potential as optical probes and gene delivery vehicles in vitro. Advantages of these NIRQDs are numerous: Highest quantum yield reported until now (150 %) may allow reduction of necessary dose for signal detection. Strong luminescence in the NIR-I window eliminates autofluorescence for better signal-to-noise ratio and allows strong optical signal. Although PEI coating provided poorly luminescent particles, incorporation of 2MPA as a co-stabilizer, provided a synergy and produced colloidally stable particles with strong luminescence and smaller size crystals compared to PEI or 2MPA coated particles. Although a polymeric coating usually provides colloidal stability, it leaves defects on crystal surface and causes poor luminescence due to the lack of dense packing restricted by the polymer backbone. Hence, addition of small strongly binding 2MPA, both decreases the crystal size due to such strong Ag-thiol binding and passivates uncoordinated sites, increasing QY.

Significant advantages are gained in terms of cytotoxicity. Heavy metal related cytotoxicity was eliminated by using quite biocompatible Ag_2S semiconductor core. PEI based toxicity was reduced by surface adsorption on QD core, possibly due to the loss of some amines upon surface binding, and coexistence of 2MPA. Although not as cytocompatible as 2MPA coated Ag_2S NIRQDs, PEI/2MPA coated Ag_2S NIRQDs are cytocompatible below 5 μg Ag^+/mL (23 μg /mL QD). Achieving cytocompatibility without PEGylation of the cationic particles are very important since PEGylation does interfere with gene delivery potential and endosomal escape of the nanoparticles. Absence of ligand exchange and PEGylation steps and direct coating of the QD core with the PEI/2MPA mixture also provided small sized particles which is advantages for prolonged blood circulation or for possible active targeting applications.

These NIRQDs were internalized by HeLa and MCF-7 cells and showed strong optical signal in CLM images. Additionally, these NIRQDs successfully transfected both of these cell lines with GFP. Transfection efficiency was about 40 % following a standard protocol which shows 30 % transfection efficiency with the control PEI (linear, 25 kDa). Possibly this can be optimized further and even better efficiencies can be obtained. In the rise of Ag_2S NIRQDs, we demonstrate the synthesis of highly luminescent, cationic QDs with the best known polymeric transfection agent, PEI, and point out the promise of Ag_2S as valuable new theranostic nanoparticles.

Acknowledgement

Authors would like to thank Assoc. Prof. Ozgur Birer (Koc University, Istanbul, Turkey) for the construction of home-made PL instrument, Dr. Baris Yagci (KUYTAM, Koc University, Istanbul, Turkey) for XPS and Assoc. Prof. Mehmet Ali Gulgun (Sabanci University, Istanbul, Turkey) for TEM analysis.

Notes and references

[a]*Koc University, Graduate School of Materials Science and Engineering, Rumelifeneri Yolu, Sarıyer, 34450, Istanbul, Turkey. Fax: +90 2123381559; Tel: +902123381742; E-mail: fyagci@ku.edu.tr.*
[b]*Sabanci University, Faculty of Engineering and Natural Sciences, Molecular Biology, Genetics Biological Sciences and Bioengineering Programs, Orhanli-Tuzla, 34956, Istanbul, Turkey.*
[c]*Koc University, Department of Physics, Rumelifeneri Yolu, Sarıyer, 34450, Istanbul, Turkey.*
[d]*Koc University, Department of Chemistry, Rumelifeneri Yolu, Sarıyer, 34450, Istanbul, Turkey.*
[e]*KUYTAM, Koc University Surface Science and Technology Center, Rumelifeneri Yolu, Sarıyer, 34450, Istanbul, Turkey.*

† Footnotes should appear here. These might include comments relevant to but not central to the matter under discussion, limited experimental and spectral data, and crystallographic data.
Electronic Supplementary Information (ESI) available: [details of any supplementary information available should be included here]. See DOI: 10.1039/c000000x

1. N. Nayerossadat, T. Maedeh and P. A. Ali, *Adv Biomed Res*, 2012, **1**, 27.
2. T. G. Park, J. H. Jeong and S. W. Kim, *Advanced Drug Delivery Reviews*, 2006, **58**, 467-486.
3. C. W. Pouton and L. W. Seymour, *Advanced Drug Delivery Reviews*, 2001, **46**, 187-203.
4. J. M. Dang and K. W. Leong, *Advanced Drug Delivery Reviews*, 2006, **58**, 487-499.
5. G. A. Husseini and W. G. Pitt, *Advanced Drug Delivery Reviews*, 2008, **60**, 1137-1152.
6. I. Honoré, S. Grosse, N. Frison, F. Favatier, M. Monsigny and I. Fajac, *Journal of Controlled Release*, 2005, **107**, 537-546.

7. G.-J. Jeong, H.-M. Byun, J. M. Kim, H. Yoon, H.-G. Choi, W.-K. Kim, S.-J. Kim and Y.-K. Oh, *Journal of Controlled Release*, 2007, **118**, 118-125.
8. S. Patil, D. Rhodes and D. Burgess, *The AAPS Journal*, 2005, **7**, E61-E77.
9. Y. Lee, *Bull. Korean Chem. Soc.*, 2008, **29**, 666-668.
10. Y. Li, X. Duan, L. Jing, C. Yang, R. Qiao and M. Gao, *Biomaterials*, 2011, **32**, 1923-1931.
11. H. Duan and S. Nie, *Journal of the American Chemical Society*, 2007, **129**, 3333-3338.
12. E. Q. Song, Z. L. Zhang, Q. Y. Luo, W. Lu, Y. B. Shi and D. W. Pang, *Journal*, 2009, **55**, 955-963.
13. A. Masotti, P. Vicennati, F. Boschi, L. Calderan, A. Sbarbati and G. Ortaggi, *Bioconjugate Chemistry*, 2008, **19**, 983-987.
14. R. Aswathy, Y. Yoshida, T. Maekawa and D. S. Kumar, *Analytical and Bioanalytical Chemistry*, 2010, **397**, 1417-1435.
15. S. B. Rizvi, S. Ghaderi, M. Keshtgar and A. M. Seifalian, *Nano Rev*, 2010, **1**.
16. Y. Lu, Y. Su, Y. Zhou, J. Wang, F. Peng, Y. Zhong, Q. Huang, C. Fan and Y. He, *Biomaterials*, 2013, **34**, 4302-4308.
17. Y.-H. Chien, Y.-L. Chou, S.-W. Wang, S.-T. Hung, M.-C. Liau, Y.-J. Chao, C.-H. Su and C.-S. Yeh, *ACS Nano*, 2013, **7**, 8516-8528.
18. J. O. Escobedo, O. Rusin, S. Lim and R. M. Strongin, *Current Opinion in Chemical Biology*, 2010, **14**, 64-70.
19. B. L. Wehrenberg, C. Wang and P. Guyot-Sionnest, *The Journal of Physical Chemistry B*, 2002, **106**, 10634-10640.
20. L. Bakueva, I. Gorelikov, S. Musikhin, X. S. Zhao, E. H. Sargent and E. Kumacheva, *Advanced Materials*, 2004, **16**, 926-929.
21. M. T. Harrison, S. V. Kershaw, M. G. Burt, A. Eychmüller, H. Weller and A. L. Rogach, *Materials Science and Engineering: B*, 2000, **69–70**, 355-360.
22. K. Schumann, *Z Ernahrungswiss*, 1990, **29**, 54-73.
23. P. Jiang, C. N. Zhu, Z. L. Zhang, Z. Q. Tian and D. W. Pang, *Biomaterials*, 2012, **33**, 5130-5135.
24. J. Chen, T. zhang, L. Feng, M. Zhang, X. Zhang, H. Su and D. Cui, *Materials Letters*, 2013, **96**, 224-227.
25. P. Jiang, Z.-Q. Tian, C.-N. Zhu, Z.-L. Zhang and D.-W. Pang, *Chemistry of Materials*, 2011, **24**, 3-5.
26. Y. Wang and X.-P. Yan, *Chemical Communications*, 2013, **49**, 3324-3326.
27. Y. Zhang, Y. Zhang, G. Hong, W. He, K. Zhou, K. Yang, F. Li, G. Chen, Z. Liu, H. Dai and Q. Wang, *Biomaterials*, 2013, **34**, 3639-3646.
28. Y. Zhang, G. Hong, Y. Zhang, G. Chen, F. Li, H. Dai and Q. Wang, *ACS Nano*, 2012, **6**, 3695-3702.
29. G. Hong, J. T. Robinson, Y. Zhang, S. Diao, A. L. Antaris, Q. Wang and H. Dai, *Angewandte Chemie International Edition*, 2012, **51**, 9818-9821.
30. H. Y. Yang, Y. W. Zhao, Z. Y. Zhang, H. M. Xiong and S. N. Yu, *Nanotechnology*, 2013, **24**, 055706.
31. M. Yarema, S. Pichler, M. Sytnyk, R. Seyrkammer, R. T. Lechner, G. Fritz-Popovski, D. Jarzab, K. Szendrei, R. Resel, O. Korovyanko, M. A. Loi, O. Paris, G. Hesser and W. Heiss, *ACS nano*, 2011, **5**, 3758-3765.
32. Y. Du, B. Xu, T. Fu, M. Cai, F. Li, Y. Zhang and Q. Wang, *Journal of the American Chemical Society*, 2010, **132**, 1470-1471.
33. C. Li, Y. Zhang, M. Wang, Y. Zhang, G. Chen, L. Li, D. Wu and Q. Wang, *Biomaterials*, 2014, **35**, 393-400.
34. G. Chen, F. Tian, Y. Zhang, Y. Zhang, C. Li and Q. Wang, *Advanced Functional Materials*, 2014, **24**, 2481-2488.
35. I. Hocaoglu, M. N. Çizmeciyan, R. Erdem, C. Ozen, A. Kurt, A. Sennaroglu and H. Y. Acar, *Journal of Materials Chemistry*, 2012, **22**, 14674.
36. S. Celebi, A. K. Erdamar, A. Sennaroglu, A. Kurt and H. Y. Acar, *The Journal of Physical Chemistry B*, 2007, **111**, 12668-12675.
37. H. Y. Acar, R. Kas, E. Yurtsever, C. Ozen and I. Lieberwirth, *Journal of Physical Chemistry C*, 2009, **113**, 10005-10012.
38. A. M. Smith, H. Duan, M. N. Rhyner, G. Ruan and S. Nie, *Physical Chemistry Chemical Physics*, 2006, **8**, 3895-3903.
39. H. Li, W. H. Shih, W. Y. Shih, L. Chen, S. J. Tseng and S. C. Tang, *Nanotechnology*, 2008, **19**, 475101.
40. A. M. Mohs, H. Duan, B. A. Kairdolf, A. M. Smith and S. Nie, *Nano Res*, 2009, **2**, 500-508.
41. Y. Zhang, J. M. Liu and X. P. Yan, *Anal Chem*, 2013, **85**, 228-234.
42. G. H. Au, W. Y. Shih, S. J. Tseng and W. H. Shih, *Nanotechnology*, 2012, **23**, 275601.
43. A. Zintchenko, A. S. Susha, M. Concia, J. Feldmann, E. Wagner, A. L. Rogach and M. Ogris, *Mol Ther*, 2009, **17**, 1849-1856.
44. A Guide to Recording Fluorescence Quantum Yields http://www.horiba.com/fileadmin/uploads/Scientific/Documents/Fluorescence/quantumyieldstrad.pdf).
45. H. Li, W. Y. Shih and W.-H. Shih, *Industrial & Engineering Chemistry Research*, 2007, **46**, 2013-2019.
46. S. Choosakoonkriang, B. A. Lobo, G. S. Koe, J. G. Koe and C. R. Middaugh, *Journal of Pharmaceutical Sciences*, 2003, **92**, 1710-1722.
47. J. D. Ziebarth and Y. Wang, *Biomacromolecules*, 2010, **11**, 29-38.
48. A. von Harpe, H. Petersen, Y. Li and T. Kissel, *Journal of Controlled Release*, 2000, **69**, 309-322.
49. H. Y. Acar, S. Celebi, N. I. Serttunali and I. Lieberwirth, *J Nanosci Nanotechnol*, 2009, **9**, 2820-2829.
50. O. Madelung, *Semiconductors: Data Handbook*, Verlag Berlin Heidelberg Newyork: Springer, 2004.
51. R. Chen, N. T. Nuhfer, L. Moussa, H. R. Morris and P. M. Whitmore, *Nanotechnology*, 2008, **19**, 455604.
52. J. Li, W. Tang, H. Yang, Z. Dong, J. Huang, S. Li, J. Wang, J. Jin and J. Ma, *RSC Advances*, 2014, **4**, 1988.